Effects of Diameter on the Durability of Glass-Fiber-Reinforced-Polymer (GFRP) Bars Conditioned in Alkaline Solution

Brahim Benmokrane,[1] Allan Manalo,[2] Jean-Charles Bouhet,[3] Khaled, Mohamed[4], and Mathieu Robert[5]

ABSTRACT

Current standards do not consider the diameter of glass-fiber-reinforced-polymer (GFRP) bars used as internal reinforcement in concrete structures to be a factor influencing bar durability. This paper investigates the effects of bar diameter on the physical and mechanical properties as well as the durability of GFRP reinforcing bars conditioned for three months at 60°C in an alkaline solution simulating a concrete environment. Five diameters (nominal diameters of 9.5 mm, 12.7 mm, 15.9 mm, 19.1 mm, and 25.4 mm) were considered; bar properties were assessed before and after conditioning. Microstructural analyses and measurement of physicochemical properties were also carried out. The results show that bar size had no significant effect on bar physical properties, except for water absorption. The smaller diameter bars had higher water absorption than the larger ones due to their higher surface-area-to-volume ratios. In the case of the unconditioned bars, the tensile strength and modulus were not significantly affected by bar diameter, but there was a size effect for interlaminar shear strength and flexural strength. On the other hand, the conditioning in the alkaline solution had a greater negative effect on the tensile strength of the larger bars than on the smaller ones. Scanning-electron-microscope (SEM) observations and Fourier-transform-infrared-spectroscopy (FTIR) analysis revealed that the degradation remained at the surface of all the conditioned specimens. Nevertheless, there were only small variations between the physical and mechanical properties of the GFRB bars of

different diameters. This indicates that the current provisions in standards that do not relate strength-retention limit to bar size are acceptable.

Keywords: GFRP reinforcing bars; diameter; durability; mechanical; properties retention; alkaline environment, concrete

[1]Professor, Canada Research Chair in Advanced Composite Materials for Civil Structures, NSERC Research Chair in Innovative FRP Reinforcement for Concrete Infrastructures, Department of Civil Engineering, University of Sherbrooke, Sherbrooke, Quebec, Canada, J1K 2R1, Phone: 819-821-7758, Fax: 819-821-7974, E-mail: Brahim.Benmokrane@USherbrooke.ca

[2]Senior Lecturer, Centre for Future Materials, Faculty of Health, Engineering and Sciences, University of Southern Queensland, Toowoomba, Queensland 4350, Australia. E-mail: Manalo@usq.edu.au

[3]M.Sc Candidate, Department of Civil Engineering, University of Sherbrooke, Sherbrooke, Quebec, Canada J1K 2R1, E-mail: jc.bouhet@hotmail.fr

[4]Postdoctoral Fellow, Department of Civil Engineering, University of Sherbrooke, Sherbrooke, Quebec, Canada J1K 2R1, E-mail: Khaled.Mohamed@usherbrooke.ca

[5]Professor, Dept. of Civil Engineering, Univ. of Sherbrooke, QC, Canada J1K 2R1. E-mail: Mathieu.Robert2@usherbrooke.ca

INTRODUCTION

Glass fiber-reinforced-polymer (GFRP) bars have emerged as an attractive alternative to steel reinforcement in concrete structures because of their corrosion performance in aggressive environmental conditions. These composite reinforcing bars have attracted significant interest because of their superior properties such as light weight, high mechanical properties, and neutrality with respect to electrical and magnetic disturbances. The results of several experimental studies, establishment of materials specifications, publication of design codes and guidelines, and successful field applications in concrete structures have driven the worldwide use and acceptance of GFRP bars (ACI 440.1R, CSA S6, CSA S806, CSA S807, fib 2007, Benmokrane et al. 2006; Drouin et al. 2011, Manalo et al. 2014; Mohamed and Benmokrane, 2016 & 2015, Arafa et al, 2016, Ahmed et al., 2016). As a result, a variety of GFRP bars manufactured with various fibers and resins as well as various surface geometries are now commercially available (ACI 440.1R). Like steel reinforcement, GFRP bars are available in diameters ranging from 6 mm to 36 mm (ACI 440.1R); larger diameter bars can be also manufactured. Unlike steel reinforcement, whose properties can be assumed to be the same for different bar diameters, GFRP bars are size dependent in terms of longitudinal strength due to shear-lag effect (Bank 2006). To illustrate, Hollaway (2008) measured a reduction in tensile strength of up to 40% when the bar diameter increased from 9.5 mm to 20 mm. For these reasons, manufacturers are required to fully report the characteristic strength, stiffness, physical, and durability properties for every type and size of FRP bar.

The mechanical, physical, and durability characteristics are important information needed in the material specifications and design of FRP bars. These properties should be determined in accordance with the prescribed test standards and methods (ACI 440.6, CSA S807). They must

also be made available to design engineers, asset owners, and building-code and standard-writing authorities (Micelli and Nanni 2004). More importantly, the physical, mechanical, and durability properties of every commercially available and newly developed GFRP bar should comply with the limits specified in the current standards and specifications (ACI 440.6, CSA S807). While the minimum specified mechanical properties are available for each bar diameter, the current ACI and CSA standards and specifications (ACI 440.6, CSA S807) do not relate the requirement limits in terms of physical and durability properties to FRP-bar size. This is because there have been few studies investigating the effect of GFRP-bar size on physical and durability properties.

The durability of GFRP bars is a complex problem because it depends upon the components of the composite material (Bakis, 1993, Benmokrane and Rahman 1998, Hollaway 2010). In particular, the reaction of GFRP bars to the alkali in concrete has received significant attention due to their importance in construction applications (Porter et al. 1997, Bakis et al. 1998, Nkurunziza et al. 2005, Chen et al. 2007, Robert et al. 2013, Belarbi and Wang 2012, Kamal and Boulfiza 2011). As internal reinforcement, FRP bars are embedded in a cementitious environment aggressive to glass FRPs (GFRPs) due to the high pH level of the pore-water solutions and the presence of alkali ions (Porter et al. 1997, Micelli and Nanni 2004, Robert et al. 2009). Most of the cases available to date focusing on the physical and durability properties of GFRP bars have involved small-diameter bars. Tannous and Saadatmanesh (1999) investigated the durability characteristics of 10 mm and 19.5 mm diameter vinyl ester and polyester-based AR-Glass FRP bars. Their results showed very small changes in the elastic modulus (0% to 2%). The tensile strength retained after 6 months exposure to an alkaline solution (pH=12) at 60 ^{o}C was only 72% to 77% for 10 mm bars, but 83% to 86% for 19.5 mm diameter bars. Furthermore, they indicated that vinyl ester provided better protection to fibers against chemical attack than

polyester. Similarly, Micelli and Nanni (2004) investigated the durability of GFRP rods subjected to alkaline exposure and high temperature (60 ^{o}C). While they considered two different diameters of GFRP rods, the 12 mm diameter bars were made from thermoplastic resin, while the 6.35 mm diameter bars were made from polyester resin. Their results revealed no degradation in the GFRP bars made with thermoplastic resin, but a reduction in tensile strength of up to 40% in the bars made with polyester resin after 42 days. Robert et al. (2009) conducted an accelerated aging test of 12.7 mm vinylester based GFRP bars with a fiber content of 77.9% by weight embedded in concrete. They found that the GFRP bars in alkaline solution experienced strength losses more than 3 times that of the GFRP bars aged in moist concrete. Most recently, Benmokrane et al. (2015) conducted a comparative durability study of 6 mm glass/vinylester, basalt/vinylester, and basalt/epoxy FRP bars. Their test results revealed that basalt/epoxy FRP bars has better mechanical property retention than basalt/vinylester. The results from these studies primarily provide the basis which the current design guidelines and codes can use in developing generalized requirement limits as well as similar environmental reduction factors for all GFRP-bar sizes. Clearly, there is a gap in research investigating the durability characteristics of GFRP bars of different sizes and correlating them with their important physical and mechanical properties.

This paper systematically investigates the physical and mechanical properties of GFRP bars of different diameters. It aims to correlate the physical and long-term characteristics of FRP bars with bar diameters for their effective use and to provide guidance in the development of design codes and material specifications for this reinforcing material. In the first stage, the physical and chemical properties of the unconditioned bar materials were determined. In the second stage, the GFRP bars were exposed to alkaline solution for 3 months at 60^{o}C to simulate the concrete pore

environment. Mechanical characterization of these conditioned bars was then conducted and compared to that of the unconditioned bars. Microstructural analyses and measurements of the physicochemical properties were also carried out on the conditioned and unconditioned GFRP bars. The findings from these studies are provided in this paper.

EXPERIMENTAL PROGRAM

Materials

The sand-coated GFRP bars used in this study were made of continuous boron-free glass fibers (EC-R) impregnated in a vinylester-based resin matrix and were manufactured according to the pultrusion process by a Canadian company (Pultrall Inc., Thetford Mines, Quebec). Five diameters of GFRP bars were investigated (#3, #4, #5, #6, and # 8), which correspond to nominal diameters of 9.5 mm, 12.7 mm, 15.9 mm, 19.1 mm, and 25.4 mm, respectively, as shown in Figure 1. The technical specifications for these bars can be found in the data sheets reported by Pultrall (2012).

Specimen Details

The preparation of specimens and characterization of the physical and mechanical properties of the GFRP bars were performed according to the appropriate ASTM, ACI, and CSA test standards. Table 1 summarizes the test methods as well as the number of specimens tested for each type of test and bar size. The specimens were cut and prepared in accordance with the recommendation of the appropriate test standards.

Bar Conditioning

The GFRP bars were separated into two series. The first series consisted of unconditioned reference bars; the second comprised GFRP bars conditioned in an alkaline solution for 90 days at 60°C. The alkaline solution used comprised 118.5 g of $Ca(OH)_2$, 0.9 g of NaOH, and 4.2 g of

KOH for 1 L of water. The solution had a pH of 12.6, which is representative of a mature concrete pore solution. The conditioning temperature was set at 60°C, as specified in ASTM D7705/D7705M-12 (2012). The conditioning was conducted in accordance with ACI 440.3R-12 (2012), Test method B.6, and CSA-S806-12 (2012), Annex O. During conditioning, the level of alkaline solution and pH level were checked periodically, and new solution added as necessary.

PHYSICAL PROPERTIES OF THE GFRP BARS

Table 2 summarizes the physical properties of the GFRP bars. The values listed within parentheses represent the standard variation of the test results.

Actual Cross-Sectional Area by Immersion Test

The actual cross-sectional area of the GFRP bars was measured in accordance with CSA-S806 (2012), Annex A. A plastic cylinder and a scale capable of measuring weight up to an accuracy of 1 g were used. Twenty-four 270 mm long specimens were prepared for each bar diameter and tested. All specimens were kept in the test environment for 24 hours prior to weighing and measuring. All the bars are oversized when compared to their respective nominal cross-sectional areas (Table 2). The average measured oversize varied from 9% to 18%, as seen with the largest (#8) and smallest (#3) bars, respectively. This variation is due to the ratio difference of the sand coating to the core. According to the average measured surface area, all bar diameters meet the Grade III requirements of the Ministry of Transport Ontario's special provision for glass-fiber-reinforced-polymer reinforcing bar.

Fiber Content

The fiber content of the GFRP bars was calculated according to ASTM D3171-15 (2015). Nine specimens for each bar diameter were identified, dried, and weighted. The bars were then placed in an oven at 650^{o}C until the polymer matrix was entirely removed by combustion. The

remaining fibers were weighed in order to get the fiber weight ratio. Since the bars were sand coated, the weight of the sand was measured separately and subtracted from the initial weight. Table 2 shows that the fiber content increased slightly with bar diameter, from 80.9% of fibers by weight for the #3 bars to 83.0% for the #8 bars. It should be noted, however, that the limits specified in CSA S807 (2010) for the glass fiber fraction by weight is only 70%.

Transverse Coefficient of Thermal Expansion

The transverse coefficient of thermal expansion was calculated according to ASTM E1131-08 (2014). Nine specimens were tested for each bar diameter. The measurements were conducted between -30°C and 60°C at a heating rate of 3°C. A TA Q400 thermomechanical analyser was used. Cryogenic equipment (liquid nitrogen) was used to reach subzero temperatures. The results show that the coefficients of thermal expansion for the different bar diameters fall between 20.5×10^{-6}/°C and 22.0×10^{-6}/°C, which is only half of the limit of 40.0×10^{-6}/°C specified in CSA 807 (2010).

Void Content

The void content of the GFRP bars was measured with the wicking test according to ASTM D5117-09 (2009). Five specimens 25 mm in length for each bar diameter were placed into a dye penetrant solution from a mixture of basic fuchsin ($C_{20}H_{19}N_3HCl$) and methyl hydrate with a 1:100 weight ratio. The wicking action is revealed by the apparition of spots on the side of the specimen not immersed in the solution. The tests were made at a room temperature and relative humidity of 23ºC and 50%, respectively. Before the test, a precautionary nail-polish shield recommended by ASTM D2374-05 (2011) was applied in order to prevent wicking along the bar periphery. The dye penetrant solution is poured in a disposable pan so that only the bottom three mm of the specimens is immersed. The presence and number of the colored dots were then noted

after 15 minutes of immersion. No colored dots were observed in any of the specimens, indicating that there were no voids or cracks running through the length of the bars. As specified in CSA 807 (2010), the void content in FRP bars should be no greater than 1%.

Water Absorption

The water absorption of the bars after 24 hours and at saturation was determined according to ASTM D 570-98 (2010). Nine specimens 75 mm in length were prepared, dried, and weighed for each bar diameter. These specimens were then entirely immersed in distilled water at 60°C. The samples were removed from the water after 24 hours, surface dried, and weighed. Then, they were placed in water again until full saturation, i.e., when the weight increase in three consecutive weightings was less than 1%. In calculating the water absorption, the loss of sand coating was considered by weighing the specimens two times, i.e., just after removing the specimens from water and after 24h of oven drying at 60°C. The difference between the two measurements gave the real mass of absorbed water.

The water absorption of the GFRP bars at 24 hours and at saturation was found to decrease as the diameter of the bars increased. The maximum absorption of the #3 bars after 24 hours and at saturation was 0.152% and 0.195%, respectively. This low water absorption for the GFRP bars considered herein—even at saturation—is due to the low moisture diffusion of the vinylester resin, as indicated by Tannous and Saadatmanesh (1999). For FRP reinforcing bars, the limit of water absorption after 24 hours specified in CSA-S807 (2010) is 0.25%. The values at saturation are 1% and 0.75% (high durability) in ACI 440.6M (2008) and CSA-S807 (2010), respectively. This shows that the water absorption of the GFRP bars with different diameters is well within the allowable specified limit in current standards.

Cure Ratio (%) and Glass Transition Temperature (T_g)

The cure ratio and glass transition temperature, T_g, of the GFRP bars were determined by differential scanning calorimetry (DSC) according to the ASTM E 1356-08 (2014) test method. For this test, nine pieces weighing about 20 mg were cut from the center of the core of each bar, weighed, and placed in an aluminum pan. The specimens were then heated from 25°C to 180°C at a rate of 10°C/min. The T_g obtained for all bar diameters ranged from 105ºC to 125ºC for the GFRP bar, which is higher than the limit of 100°C specified in CSA S807 (2010) and ACI 440.6M (2008). Similarly, a cure ratio of 100% was measured for all bar diameters. It is worth noting that the specified cure ratio for GFRP bars is only 95% (CSA S807, 2010).

MECHANICAL PROPERTIES OF THE GFRP BARS

The mechanical properties of the unconditioned (reference) and conditioned GFRP bars with different diameters were assessed under three-point flexural testing, short-beam shear testing, and tensile testing. Due to the limited length of both the conditioned and unconditioned #6 GFRP bar specimens provided by the industry partner, there were no remaining portions to conduct the flexural testing for this bar size. Table 3 summarizes the results of the mechanical characterization. The values listed within parentheses are the standard deviation of the test results. The nominal diameter and nominal cross-sectional area of the GFRP bars were used in calculating the mechanical properties.

Flexural Properties

Flexural testing was conducted for comparative assessment of the mechanical properties of the FRP bars. The test was conducted in accordance with ASTM D4476/D4476M-14 (2014). The unconditioned and conditioned specimens were tested over a simply supported span equal to 20 times the bar diameter and with an overhang twice the bar diameter at each support. Six

replicates for each bar diameter were tested under laboratory conditions on an MTS 810 testing machine equipped with a 500 kN load cell. The specimens were loaded at the midspan with a circular nose and supported at the ends on two circular supports that allowed the specimens to bend, as shown in Figure 2a. A displacement control rate of 3.0 mm/min was used. The applied load and deflection were recorded during the test with a data acquisition system monitored by a computer. The flexural strength of the GFRP bars, f_u, in the outermost fibers at midspan was calculated as $f_u = PLc/(4I)$, where P is the failure load, L is the clear span, c is the distance to the centroid of the extreme-most fibers, and I is the moment of inertia.

Under bending, the load–deflection behavior of all the specimens (Figure 3a) showed linear behavior, but a slight reduction in stiffness was observed before final failure. This reduction of stiffness is due to the initiation of compressive failure under the loading point, which is more noticeable in the conditioned specimens than the reference samples. Moreover, the conditioned samples failed at lower load and deflection than the reference samples, but with the same bending stiffness prior to failure. Regardless of diameter, the bars failed due to compression in the top fibers, followed by tensile failure at the bottom near the midpoint of the specimens (Figures 3b and 3c).

Interlaminar Shear-Strength Properties

The short-beam shear testing was conducted following ASTM D4475-02 (2016) in order to determine the interlaminar shear strength of FRP bars (Figure 2b). The short-beam shear test is a matrix-dominated property and can give an indication of the resistance of the fiber–matrix interface. The test was carried out with MTS 810 testing machine equipped with a 500 kN load cell. Six replicates for each bar diameter were prepared and tested. The distance between the shear planes was set to six times the nominal diameter of the FRP bars. A displacement control

253 rate of 1.3 mm/min was employed for the #3, #4, and #5 bars, while 1.8 mm/min was used for
254 the #6 and #8 bars. The applied load and displacement were recorded with a computer-monitored
255 data-acquisition system. The interlaminar shear strength S_u of the FRP bar was calculated as
256 $S_u = 0.849P/d^2$, where P is the shear failure load and d is the bar diameter.

257 Figure 4 shows the results from short-beam shear testing. It can be seen that the applied load
258 increased linearly with the deflection with a slight nonlinearity before the final failure. This
259 nonlinear behavior before final failure is more apparent in the larger diameter bars. The
260 experimental results also show that the conditioned specimens failed at a lower load than the
261 reference samples. Micelli and Nanni (2004) indicated that the decrease in the apparent
262 horizontal shear strength of the conditioned GFRP bars is caused by resin damage due to
263 penetration of the alkaline solution. Both the unconditioned and conditioned specimens failed
264 due to horizontal shear cracks that originated from the edge of the bars and developed along the
265 length (Figures 4b and 4c). Park et al. (2008) indicated that very high interlaminar-shear stresses
266 can arise at the free edge of fiber composite materials. The only observed difference was the
267 more obvious compressive failure under the loading point and at the supports that occurred with
268 the larger diameter bars. This is due to the higher load needed to cause failure of the larger
269 diameter bars and achieve the same level of interlaminar shear stress, while the contact area
270 under the loading point was almost the same for all of the bar sizes. This observation explains the
271 nonlinear behavior of the bars before the final failure.

272 **Tensile Properties**

273 Tensile testing was conducted according to ASTM D7205/D7205M-06 (2011) and CSA-S806-12
274 Annex C. The tensile testing along the alignment of fibers is related to fiber properties. The
275 gauge length of the specimens was approximately equal to 40 times the bar diameter, in addition

to the length of the anchorage steel tubes at each end of the GFRP bars, as specified in CSA-S806-12, Annex B. Table 4 provides the specimen and anchor length for each bar size. Each specimen was instrumented with two LVDTs 200 mm in length to capture specimen elongation during testing (Figure 1c). To avoid damaging the LVDTs, they were detached from the specimen when the load reached 75% of the estimated ultimate load. The tests were carried out with a Satec-Baldwin testing machine equipped with a 2000 kN load cell. The load was increased at a rate of 300 MPa/min until tensile failure occurred. Six specimens were tested for each bar diameter. The applied load and bar elongation were electronically recorded during the test with a computerized data-acquisition system. This test determined the ultimate tensile strength f_t, tensile modulus E and tensile strain ε.

The typical stress strain behavior of the GFRP bars with different diameters is shown in Figure 5a. All of the specimens behaved in a linear elastic fashion in tension up to failure and exhibited almost identical slopes in the stress–strain curve. It is to be noted that the strain after the LVDT's were removed was calculated based on the stress and elastic modulus of the bars. This behavior indicates that the elastic moduli of the bars with different diameters were similar and that the loss of elastic modulus due to exposure to the simulated alkaline environment was negligible. Nevertheless, the failure stress and rupture strain of the conditioned bars were lower than that of the reference bars. Robert et al. (2009) had similar findings and they indicated that the elastic modulus of the GFRP bars they tested was not affected by aging in a concrete environment, but tended to be more brittle and evidenced lower strength than the reference bars. Generally, rupture strain decreases as bar diameter increases. Figures 5b and 5c show that, regardless of diameter, the GFRP bars tested failed at the middle of the bar (within the gauge length). All of the specimens failed suddenly, as expected, due to tensile fiber rupture. Prior to

failure, a popping noise was heard caused by some of the fibers and/or the resin failing on the outer perimeter of the bar. It is important to note that the measured tensile strength for both the reference and conditioned bars (all bar diameters) was significantly higher than 655 MPa and 750 MPa, and that their elastic moduli were 39.3 GPa and 60 GPa, as specified in ACI 440.6M and CSA S807-10, respectively for high modulus GFRP bars. Similarly, the failure strain was higher than the prescribed 1.2%.

DISCUSSION

The effects of bar diameter on physical, mechanical, and durability properties are analyzed and discussed in this section.

Effect of Bar Diameter on Physical Properties

The bar diameter had no significant effect on most of the physical properties of the GFRP bars, including the transverse coefficient of thermal expansion, porosity, and T_g. Similarly, all of the bars tested evidenced an entirely cured resin, indicating that bar diameter did not affect the degree of cure. The development of an efficient production method makes this consistency possible. This is in contrast with the observations made by Yi and Hilton (1988), who indicated that laminate thickness might affect the degree of cure due to the higher thermal conductivity of thicker composite laminates. On the other, the fiber content and water absorption were found to increase and decrease, respectively, with increasing bar diameter. Since none of the FRP bars contained voids, the lower water absorption for the larger diameter bars can be correlated to increasing fiber content (by weight), as noted in section 2.4.1. Glass fibers absorb scarcely any water, therefore the bars with higher matrix contents evidenced higher absorption rates.

In order to further correlate bar diameter to the percentage water absorption, the shape ratio of the GFRP bars were calculated and plotted (see Figure 6). Cinquin and Medda (2009) defined the

shape ratio as the ratio between the sample's surface and volume. As can be seen in Figure 6a, the shape ratio was significant in the water absorption of the GFRP bars at 24 hours (*24 h*) and at saturation (*Saturation*), i.e., the water absorption increased as did the shape ratio. It can also be observed that the relationship between the water absorption at 24 hours (%) and at saturation to that of the shape ratio is the same, as demonstrated by the almost equal slopes of the water absorption and shape-ratio relationship curves. On the another hand, there is a linear but negative correlation between the shape ratio and bar diameter. The shape ratio decreases as the bar diameter increases. This accounts for the smaller diameter bars having higher absorption rates than the larger diameter ones with the same length, since the exposed surface is greater with respect to volume. It is also worth noting that the decrease in the shape ratio is very similar to the decrease in the percentage of water absorption at saturation (%) for the various bar diameters.

Effect of Bar Diameter on Mechanical Properties

Many studies have revealed that the short-term mechanical properties of FRP bars decrease with increased bar diameter (Bank 2006; Hollaway 2008). This conclusion, however, was not clearly observed in our study. Figure 7 shows the normalized mechanical properties for the different sizes of GFRP bars. This graph provides the percentage of the interlaminar shear strength (*ILSS*), flexural strength (*Flexure*), tensile strength (*Tensile*), and tensile modulus (*Modulus*) for all of the bar diameters with respect to the mechanical properties of the #3 bars. The figure show no significant difference in the tensile properties of the GFRP bars regardless of bar diameter. While the highest tensile strength and modulus were observed for the #3 bars, the lowest tensile properties were exhibited by the #5 bars (94% compared to the #3 bars), with the #8 bars exhibiting more than 96% of strength and stiffness of the #3 bars. Kocaoz et al. (2005) suggested that modulus, which is an intrinsic property of the material, is not significantly affected by bar

cross-sectional size but rather by the level of fibers contained in the bar. Since the percentage fiber content by weight (%) (Table 2) for different bar diameters was almost the same, then the bars should record the same elastic modulus. Moreover, the consistency in the measured tensile properties of the GFRP bars with different diameters can be due to an adequate anchor length, which resulted in a more efficient transfer of stresses from the bar surface to the center. Portnov and Bakis (2008) suggested that introducing a more uniform distribution of the applied shear stress near the grips could minimize the shear lag effect and increase the tensile-load-carrying capacity of round pultruded rods.

In contrast to the tensile properties, there was a size effect observed for ILSS and flexural strength. The #8 bars recorded ILSS and flexural strength almost 14% lower than the #3 bars. Significant size effects were also observed by Wisnom and Jones (1996) on the average ILSS for unidirectional glass-fiber/epoxy composites. They indicated that the lower ILSS with bigger specimens could be due to the larger inherent defects. Koller et al. (2007) also suggested that the probability of having large defects in composite materials increases with increased specimen volume. Moreover, it should be noted that ILSS is a matrix-dominated property. Wisnom and Jones (1996) suggested that matrix-dominated failures show the largest size effects in composite materials. Defects near the edge of the GFRP bars were very critical for the specimens subjected to the short-beam test as this location is subjected to higher levels of shear stress. Similarly, the lower flexural properties of the larger diameter bars can be explained by the high probability of defects. Carvelli et al. (2009) suggested that it is more difficult to keep the filaments parallel to one another in larger diameter FRP bars during the pultrusion process, increasing their tendency to buckle under compression. This is, in fact, the failure mechanism observed in the GFRP bars

during the flexural test, in which the failure was initiated by the compression buckling of the top fibers.

Property Retention of GFRP bars with Different Diameters

Tannous and Saadatmanesh (1999) indicated that the effect of an alkaline solution on FRP bars only involved a very thin layer on the exposed surface. Thus, the approximate layer thickness and area of the GFRP bars affected by the alkaline solution were calculated and reported in Table 5 to correlate with the property retention for different bar diameters. These values were determined by assuming that the affected portions of the GFRP bar were the same as the percentage of water absorption at saturation (%) and equally distributed along the surface of the bars (Table 2). This approach was similar to the method adopted by Cinquin and Medda (2009). It can be clearly seen that the affected thickness is only in the order of 1.9×10^{-3} to 5.4×10^{-3} mm. Moreover, the percentage of affected thickness with respect to the nominal diameter decreased as did bar diameter.

Figure 8 provides the strength and stiffness retention properties of the GFRP bars with different diameters. Figures 8a to 8c clearly indicate that the strength properties were affected by conditioning in the alkaline solution, while Figure 8d shows that the modulus of elasticity was not affected. The almost 100% retention of the modulus of elasticity, which is a fiber-dominated property, for all bar diameters indicates that the damage caused by the moisture diffusion was confined to the very thin layer of the exposed surface and that the reinforcing fibers were not affected by the conditioning. As the modulus of elasticity was determined from the linear-elastic portion of the stress and strain curve, the matrix was still effectively transferring stresses to the fibers. Nkurunziza et al. (2005) indicated that the diffusion of moisture and alkalis in composites can destroy the bond between the fiber and matrix, damaging the interface. This is difficult to see

at lower loads, but higher mechanical loads increase the degradation of the fiber–matrix interface. This accounts for the noticeable decrease in strength properties, as these values were calculated at the point of failure of the GFRP bars at which the stress distribution along the fibers is less uniform.

Figures 8a shows that the effect of conditioning on the ILSS of the GFRP bars was significant with the smaller diameter bars, but decreased as the diameter increased. In fact, the residual horizontal shear strength for the #8 bars was the same as that measured on the reference bars, while the #3 bars retained only 88% of their ILSS. This can be explained by the thinner layer affected by the alkaline solution in the case of the larger diameter bars, as reported in Table 5. As indicated in the previous section, ILSS is governed by the fiber–matrix interface. Thus, the decrease in ILSS can be correlated to interface degradation. Similarly, due to the very thin layer affected by conditioning in the alkaline solution in the larger diameter GFRP bars, its affected area was also significantly smaller with respect to the total area, compared to the smaller diameter bars.

Figure 8b shows that the flexural-strength retention increased with bar diameter. The retention ranged from 88% retention for the #3 bars to more than 97% for the #8 bars. This behavior was also observed by Maranan et al. (2014), who found that larger diameter bars exhibited a slower rate of strength degradation at high temperature than small diameter bars. Cinquin and Medda (2009) also concluded that the residual mechanical properties were more affected in thin composites than thick composites. The higher flexural strength retention for the larger diameter bars could be due to the strength gradient through bar diameter during bending. During flexural tests, the outermost fibers are subject to the maximum stress. Thus, a smaller amount of fibers with respect to the total volume was under the maximum stress in the larger diameter bars.

Moreover, the higher flexural-strength retention in the larger diameter bars can be correlated to the smaller reduction in the second moment of area of the conditioned specimens. Since only the bar surface was damaged, the fibers and matrix in the intact zone were undamaged and had the same initial mechanical properties, resulting in a better redistribution of load when the outer fibers progressively failed.

Figure 8c shows a opposite trend than do Figures 8a and 8b, in which the smaller diameter bars exhibited higher tensile-strength retention. This figure shows that the #3 bars retained more than 95% of their tensile strength, while the #8 bars retained only 88%. This trend can be due to the shear lag effect. Achillides and Pilakoutas (2004) indicated that larger diameter FRP bars had more significant shear lag-effect than smaller diameter bars and had a noticeable effect on tensile strength. Castro and Carino (1998) further mentioned that the efficiency of the stress transfer from the bar surface to the interior fibers influences the mechanical properties of the FRP bars. Due to the shear lag effect, the outer fibers experience higher stresses than the inner fibers, even though all fibers resist the tensile load at the same time. Due to conditioning in alkaline solution, the outer surface of the bars was affected and might have decreased mechanical properties. As the specimens were loaded, the outer fibers— which were subjected to higher stress—initiated failure and the breakage moved instantly to the inner fibers, leading to the sudden and catastrophic failure of the GFRP bars. This also explains the reason why the tensile strength is more affected by the conditioning than the interlaminar shear and flexural strength.

From the above results, it can be concluded that the conditioning in alkaline solution affected the flexural, ILSS, and tensile strength properties of the GFRP bars, but not their moduli of elasticity. Moreover, the strength-retention limit was affected by bar size. The ILSS and flexural strength of the smaller diameter bars was affected more than the larger diameter ones. This is in

contrast to tensile strength: the larger diameter bars had lower tensile strength retention. These results suggest that the conclusions drawn by most studies based on smaller diameter FRP bars do not apply to larger diameters. Based on the results in this study, it is more reasonable to use larger diameter bars in assessing the tensile-strength retention of FRP bars exposed to severe environmental conditions. Nevertheless, note should be taken of the very high load required to cause failure of larger bars. That notwithstanding, the strength retention in all the bar diameters considered in this study is significantly higher than the 0.70 environmental reduction coefficient required by several codes.

SEM AND FTIR OBSERVATIONS

Scanning-electron-microscopy (SEM) observations were performed to assess the microstructure of the GFRP bars before and after conditioning. All of the specimens observed under SEM were cut, polished, and coated with a thin layer of gold–palladium using a vapor-deposit process. Microstructural observations were performed on a JEOL JSM-840A SEM. Similarly, Fourier Transformed Infrared Spectroscopy (FTIR) was conducted for each bar diameter to study the changes in the chemical composition of the matrix at the bar surface. These observations were conducted to determine the potential degradation of the polymer matrix, glass fibers, or interface, as applicable, due to the penetration of the alkaline solution. The aim was to link these observations to the possible evolution of mechanical properties and chemical composition of the bars after conditioning.

SEM

Figures 9 and 10 show the SEM micrographs of the cross section of the reference and conditioned GFRP bars, respectively. As shown in Figures 9a and 9b, there were no pores observed in the center or near the surface of the reference bars. There was also no noticeable gap

459 at the fiber–matrix interface, indicating excellent adhesion between the fibers and matrix. This is
460 also true in the center of the conditioned GFRP bars (Figure 10a). Small gaps between the fibers
461 and matrix were observed near the exposed surface in some conditioned specimens (Fig. 10b),
462 suggesting that the bars were affected after exposure to the alkaline solution. This damage to the
463 fiber–matrix interface reduces the transfer of loads between fibers and results in the reduction in
464 strength properties. Benmokrane et al. (2002), however, indicated that the mechanical properties
465 of GFRP bars are controlled by the fiber component. If the fibers have not deteriorated, FRP bars
466 will preserve most of their mechanical strength and will be able to support loads. If the protective
467 resin degrades, the bonding between the matrix and fibers located on the outer part of the bar will
468 gradually reduce and bar resistance will start to decrease. This is the most probable reason why
469 the flexural, ILSS, and tensile strength properties of GFRP bars decreased after alkaline
470 conditioning for 3 months. Nevertheless, the strength reduction is small as the SEM observation
471 confirmed that only the exposed surface of the GFRP bars was affected, not the core section.
472 This exposed surface can be considered as being an "all-resin" surface, which does not contribute
473 much in resisting the applied tensile load.

474 **FTIR**

475 Figure 11 shows the infrared spectroscopy (FTIR) spectra of the surface of the reference and
476 conditioned GFRP bars. Only the FTIR for the #3 and #8 bars are provided for comparison. The
477 FTIR for both bar diameters shows no clear differences between the infrared spectra of the
478 reference and conditioned GFRP bars. Moreover, the FTIR did not show any significant changes
479 in the chemical structure after exposure to the alkaline solution. These observations indicate that
480 the surface of the bars exposed to the alkaline solution for 3 months at 60^{o}C had not been
481 chemically modified and might possess the same initial mechanical properties. These results

further confirm that the degradation of the matrix remains only at the exposed surface of the GFRP bars. This supports the findings by Nkurunziza et al. (2005) that vinylester epoxies are very resistant to chemical attack, which improves the environmental resistance of FRP bars made with these resins.

CONCLUSIONS

The effects of diameter on the physical, mechanical, and durability properties of sand-coated GFRP bars made of continuous boron-free glass fibers (EC-R) impregnated in a vinylester-based resin matrix were investigated. Based on the results of this study, the following conclusions were drawn for the tested GFRP bars:

- With the bar sizes considered, bar diameter did not affect fiber content, transverse coefficient of thermal expansion, porosity, or glass transition temperature. On the other hand, the water absorption was found to decrease as the diameter increased. This can be correlated to the ratio of the surface area to the volume (shape ratio) of the GFRP bars.
- The tensile strength and modulus of the reference bars were not significantly affected by the cross-sectional size, but a size effect was observed for interlaminar shear strength and flexural strength. The consistency in the measured tensile properties for GFRP bars with different diameters is due to the efficient stress transfer from the bar surface to the center. On the other hand, the higher probability of defects contained in the larger diameter bars may have caused the lower interlaminar shear strength and flexural strength in comparison to the smaller diameter bars.
- The elastic moduli of the reference and conditioned bars were same for all bar diameters, which is due to nearly same fiber content of the GFRP bars.

- The interlaminar shear strength and flexural strength of the larger diameter GFRP bars were less affected after exposure to the alkaline solution than the smaller bar diameter. The higher interlaminar shear and flexural strength retention for the larger bar sizes was due to the lower affected thickness. As a result, the penetrated area was proportionally small relative to the total cross-sectional area of the bar.
- The tensile-strength retention was highest for the smallest diameter bar. This suggests that the impact of conditioning on the tensile properties of GFRP bars is expected to be greater for larger than smaller diameters.
- The scanning-electron-microscope and FTIR observations showed no changes in the material properties and chemical structure in the exposed surface of the bars after conditioning in the alkaline solution for 90 days at 60^{o}C. This shows that the degradation remained at the surface for all the bar diameters.

Nevertheless, the variations in the physical and mechanical properties of the GFRP bars investigated in this study, from one diameter to another, remained low. Thus, the suggestions of the current standards and specifications to not relate the strength-retention limit to the size of the FRP bars are acceptable. Further research, however, is needed to investigate other bar types and diameters to clearly determine how the diameter might affect the design of GFRP-reinforced concrete structures.

ACKNOWLEDGMENTS

The authors would like to acknowledge the support of the Natural Sciences and Engineering Research Council of Canada (NSERC), NSERC Research Chair in Innovative FRP Reinforcement for Concrete Infrastructures, The Fonds Québécois de la Recherche sur la Nature et les Technologies (FQR-NT), and Pultrall Inc. (Thetford Mines, Quebec) for the GFRP

materials support. The technical assistance from the staff of the Structural Laboratory in the Department of Civil Engineering, Faculty of Engineering at the University of Sherbrooke, are also acknowledged. The second author also acknowledges the scholarship granted by the Australian Government Endeavour Research Fellowships to undertake his research and professional development at the University of Sherbrooke.

REFERENCES

Ahmed, E., Benmokrane, B., and Sansfaçon, M. (2016). "Case Study: Design, Construction, and Performance of the La Chancelière Parking Garage's Concrete Flat Slabs Reinforced with GFRP Bars." *ASCE Journal of Composites for Construction*, DOI: 10.1061/(ASCE)CC.1943-5614.0000656

American Concrete Institute (2008). Metric specification for carbon & glass fiber-reinforced polymer bar materials for concrete reinforcement. ACI-440.6M-08, Farmington Hills, Michigan, USA.

American Concrete Institute (2012). Guide test methods for fiber-reinforced polymer, ACI 440.3R-12, Farmington Hills, Michigan, USA.

American Concrete Institute (2015). Guide for the design and construction of concrete reinforced with FRP bars, ACI 440.1R-15, Farmington Hills, Michigan, USA.

Arafa, A., Farghaly, A., Ahmed, E., Benmokrane, B. (2016). "Testing of GFRP-RC Panels with UHPRFC Joints of Nipigon River Cable Stayed Bridge in Northwest Ontario, Canada." *ASCE Journal of Bridge Engineering*, DOI: 10.1061/(ASCE)BE.1943-5592.0000943, p. 05016006-1-05016006-14.

Archillides, Z. and Pilakoutas, K. (2004). "Bond behaviour of fibre reinforced polymer bars under direct pullout conditions." *Journal of Composites for Construction*, 8(2), 173-181.

ASTM Standard D570 − 98 (2010). Standard test method for water absorption of plastics. *ASTM D570 − 98,* ASTM International, West Conshohocken, Philadelphia, Pa 19103.

ASTM Standard D2374-05 (2011). Standard test method for lead in paint driers by EDTA Method. *ASTM D2374-05,* ASTM International, West Conshohocken, Philadelphia, Pa 19103.

ASTM Standard D3171-15 (2015). Standard test methods for constituent content of composite materials. *ASTM D3171−15,* ASTM International, West Conshohocken, Philadelphia, Pa 19103.

ASTM Standard D4475-02 (2016). Standard test method for apparent horizontal shear strength of pultruded reinforced plastic rods by the short-beam method. *ASTM D4475-02,* ASTM International, West Conshohocken, Philadelphia, Pa 19103.

ASTM Standard D4476/D4476M - 14(2014). Standard test method for flexural properties of fiber reinforced pultruded plastic rods. *ASTM D4476/D4476M-14,* ASTM International, West Conshohocken, Philadelphia, Pa 19103.

ASTM Standard D5117-09 (2009). Standard test method for dye penetration of solid fiberglass reinforced pultruded stock. *ASTM D5117 − 09,* ASTM International, West Conshohocken, Philadelphia, Pa 19103.

ASTM Standard D7205/D7205M-06 (2011). Standard test method for tensile properties of fiber reinforced polymer matrix composite bars. *ASTM D7205/D7205M-06,* ASTM International, West Conshohocken, Philadelphia, Pa 19103.

ASTM Standard D7705/D7705M - 12(2012). Standard test method for alkali resistance of Fiber Reinforced Polymer (FRP) matrix composite bars used in concrete construction. *ASTM D7705/D7705M-12,* ASTM International, West Conshohocken, Philadelphia, Pa 19103.

ASTM Standard E1131-08(2014). Standard test method for compositional analysis by thermogravimetry. *ASTM E1131-08,* ASTM International, West Conshohocken, Philadelphia, Pa 19103.

ASTM Standard E1356-08(2014). Standard test method for assignment of the glass transition temperatures by differential scanning calorimetry. *ASTM E1356-08,* ASTM International, West Conshohocken, Philadelphia, Pa 19103.

Bakis, C. E. (1993) "FRP Composites: Materials and Manufacturing." *Fiber-Reinforced-Plastic for Concrete Structures: Properties and Applications*, A. Nanni, ed., Elsevier, Amsterdam, pp. 13-58.

Bakis, C. E., Freimanis, A. J., Gremel, D., and Nanni, A. (1998) "Effect of resin material on bond and tensile properties of unconditioned and conditioned FRP reinforcement rods." *Proceedings of the First International Conference on Durability of Composites for Construction*, B. Benmokrane and H. Rahman, eds., Sherbrooke, QC, Canada, pp. 525-535.

Bank, L.C. (2006). Composites for construction: Structural design with FRP materials, John Wiley and Sons, Inc., New Jersey.

Belarbi, A., and Wang, H. (2012) "Durability of FRP bars embedded in fiber-reinforced-concrete," *Journal of Composites for Construction*, 16(4), pp. 371-380.

Benmokrane, B., and Rahman, H., eds. (1998) "Durability of Fiber Reinforced Polymer (FRP) composites for construction," *Proceedings of the First International Conference (CDCC '98)*, QC, Canada, 692 pp.

Benmokrane, B., Wang, P., Ton-That, T., Rahman, H., and Robert, J.F. (2002). "Durability of glass fibre reinforcing bars in concrete environment." *Journal of Composites for Construction*, 6(3), 143-153.

Benmokrane, B., El-Salakawy, E., El-Ragaby, A., and Lackey, T. (2006). "Designing and testing of concrete bridge decks reinforced with glass FRP bars." Journal of Bridge Engineering, 11(2), 217-229.

Benmokrane, B., Elgabbas, F., Ahmed, E., and Cousin, P. (2015). "Characterisation and comparative durability study of glass/vinylester, basalt/vinylester, and basalt/epoxy FRP bars." *Journal of Composites for Construction*, 19(6):04015008, 1-12.

Canadian Standards Association (CSA). (2010). "Specification for fibre-reinforced polymers." CAN/CSA-S807, Rexdale, Ontario, Canada.

Canadian Standards Association (CSA). (2012). "Design and construction of building structures with fibre-reinforced polymers." CAN/CSA-S806-12, Rexdale, Ontario, Canada.

Canadian Standards Association (CSA). (2006-Edition 2014). "Canadian highway bridge design code—Section 16, updated version for public review." CAN/CSA-S6-14, Rexdale, Ontario, Canada.

Carvelli, V., Giulia, F., and Pisani, M.A. (2009) "Anchor system for tension testing of large diameter GFRP bars." *Journal of Composites for Construction*, 13(5), 344-349.

Castro, P.F. and Carino, N.J. (1998) "Tensile and non-destructive testing of FRP bars." *Journal of Composites for Construction*, 2(1), 17-27.

Chen, Y., Davalos, J. F., Ray, I., and Kim, H.-Y. (2007) "Accelerated aging tests for evaluations of durability performance of FRP reinforcing bars for concrete structures." *Composite Structures*, 78(1), 101-111.

Cinquin, J., and Medda, B. (2009) "Influence of laminate thickness on composite durability for long term utilisation at intermediate temperature (100 - 150^{o}C)." *Composites Science and Technology*, 69, 1432-1436.

617 Drouin, B., Latour, G., and Mohamed, H. (2011) "More than 10 years successful field
618 applications of FRP bars in Canada." *CDCC 2011, The Fourth International Conference on*
619 *Durability & Sustainability of Fiber Reinforced Polymer (FRP) Composites for Construction*
620 *and Rehabilitation,* Quebec City, QC, Canada, 6 pp.
621 *fib*, (2007) "FRP Reinforcement in RC Structures" Bulletin No. 40, Federal Institute of
622 Technology, Lausanne, Switzerland.
623 Hollaway, L.C. (2008). "Advanced fibre polymer composite structural systems used in bridge
624 engineering." *ICE Manual of Bridge Engineering,* 503-529.
625 Hollaway, L.C. (2010). "A review of the present and future utilisation of FRP composites in the
626 civil infrastructure with reference to their important in-service properties." *Construction and*
627 *Building Materials,* 24, 2419-2445.
628 Kamal, A., and Boulfiza, M., (2011) "Durability of GFRP rebars in simulated concrete solutions
629 under accelerated aging conditions." *Journal of Composites for Construction,* 15(4), pp. 473-
630 481.
631 Kocaoz, S., Samaranayake, V.A., and Nanni, A. (2005). "Tensile characterization of glass FRP
632 bars." *Composites: Part B,* 36, 127-134.
633 Koller, R., Chang, S. and Xi, Y. (2007). "Fiber-reinforced bars under freeze-thaw cycles and
634 different loading rates." *Journal of Composite Materials,* 41(1), 5-25.
635 Manalo, A.C., Benmokrane, B., Park, K., and Lutze, D. (2014). "Recent developments on FRP
636 bars as internal reinforcement in concrete structures". *Concrete in Australia*, 40(2), 46-56.
637 Maranan, G.B., Manalo, A.C., Karunasena, W., Benmokrane, B., and Lutze, D. (2014). "Flexural
638 behaviour of glass fibre reinforced polymer (GFRP) bars subjected to elevated temperature".

Proc. 23rd Australasian Conference on the Mechanics of Structures and Materials (ACMSM23), Byron Bay, Australia, 187-192.

Micelli, F., and Nanni, A. (2004). "Durability of FRP rods for concrete structures." *Construction and Building Materials*, 18, 491-503.

Mohamed, H.M., and Benmokrane, B. (2014). "Design and Performance of Reinforced Concrete Water Chlorination Tank Totally Reinforced with GFRP Bars." *ASCE Journal of Composites for Construction*, Vol. 18, No.1, pp. 05013001-1 – 05013001-11

Mohamed, H. M., and Benmokrane, B. (2015). "Make the Case: The Use of FRP Bars for Soft-Eyes in Construction of Tunnels." *Tunnels and Tunneling, The official publication of the Tunneling Association of Canada*, Dec.-Jan., pp. 35-40.

Nkurunziza, G., Debaiky, A., Cousin, P., and Benmokrane, B. (2005). "Durability of GFRP bars: A critical review of the literature." *Progress in Structural Engineering and Materials*, 7(4), 194–209.

Park, C., Jang, C., Lee, S., and Won, J. (2008). "Microstructural investigation of long-term degradation mechanisms in GFRP dowel bars for jointed concrete pavement." *Journal of Applied Polymer Science*, 108(5), 3128 -3137.

Porter, M. L., Mehus, J., Young, K. A., O'Neil, E. F., and Barnes, B. A. (1997) "Aging for Fiber Reinforcement in Concrete," *Proceedings of the Third International Symposium on Non-Metallic (FRP) Reinforcement for Concrete Structures (FRPRCS-3)*, V. 2, Japan Concrete Institute, Tokyo, Japan, pp. 59-66.

Portnov, G. and Bakis, C.E. (2008). "Analysis of stress concentration during tension of round pultruded composite rods." *Composite Structures*, 83, 100-109.

661 Pultrall (2012). V-ROD FRP reinforcing bars data sheet. Website:
662 http://www.vrodcanada.com/sites/default/files/pdfs-uploaded/V-
663 ROD%2060GPa%20Grd%20III%20Std%20-%20Oct%202012.pdf
664 Robert, M., and Benmokrane, B. (2013) "Combined effects of saline solution and moist concrete
665 on long-term durability of GFRP reinforcing bars." *Journal of Construction and Building*
666 *Materials*, 38, pp. 274-284.
667 Robert, M., Cousin, P., and Benmokane, B. (2009). "Durability of GFRP reinforcing bars
668 embedded in moist concrete." *Journal of Composites for Construction*, 13(2), 66-73.
669 Tannous, F.E. and Saadatmanesh, H. (1999). "Durability of AR glass fibre reinforced plastic
670 bars." *Composites for Construction*, 3(1), 12-19.
671 Wisnom, M.R. and Jones, M.I. (1996). "Size effects in interlaminar tensile and shear strength of
672 unidirectional glass fibre/epoxy." *Journal of Reinforced Plastics and Composites*, 15 (1), 2-15.
673 Yi, S. and Hilton, H.H. (1998). "Effects of thermo-mechanical properties of composites on
674 viscosity, temperature and degree of cure in thick thermosetting composite laminates during
675 curing process." *Journal of Composite Materials*, 32 (7), 600-622.
676

List of Tables:

List of Figures:

697 Table 1. Summary of the test methods and number of specimens

Properties	**Test Method**	**No. of Specimens**	**Reference**	**Conditioned**
Physical properties				
Cross-sectional area (mm^2)	CSA-S806, Annex A (2012)	9	√	--
Fiber content by weight (%)	ASTM D3171-15 (2015)	9	√	--
Transverse CTE, ($x10^{-6}/^oC$)	ASTM E1131-08 (2014)	9	√	--
Void content (%)	ASTM D5117-09 (2009)	9	√	--
Water absorption at 24 hours (%)	ASTM D570-98 (2010)	15	√	--
Water absorption at saturation (%)	ASTM D570-98 (2010)	15	√	--
Cure ratio (%)	ASTM E 1356-08 (2014)	15	√	--
Tg (°C)	ASTM E 1356-08 (2014)	15	√	--
Mechanical properties				
Flexure	ASTM D4476/D4476M-14 (2014)	6	√	√
Interlaminar shear	ASTM D4475-02 (2016)	6	√	√
Tensile	ASTM D7205/D7205M-06 (2011)	6	√	√

698

699

700 Table 2. Physical properties of the GFRP bars

Property	**Bar designation**				
	#3	**#4**	**#5**	**#6**	**#8**
Nominal diameter (mm)	9.5	12.7	15.9	19.1	25.4
Nominal cross-sectional area (mm^2)	70.8	126.6	198.5	286.5	506.7
Actual cross-sectional area by immersion test (mm^2)	83.8 (1.9)	145.0 (1.7)	224.4 (1.2)	317.3 (1.9)	555.7 (5.2)
Fiber content by weight (%)	80.9 (0.2)	81.8 (0.1)	82.6 (0.1)	82.7 (0.2)	83.0 (0.2)
Transverse CTE, ($x10^{-6}/^oC$)	20.7 (2.3)	20.5 (1.6)	21.5 (1.4)	22.0 (1.8)	21.3 (2.5)
Void content (%)	0 (0)	0 (0)	0 (0)	0 (0)	0 (0)
Water absorption at 24 hours (%)	0.15 (0.01)	0.12 (0.02)	0.10 (0.01)	0.02 (0.00)	0.02 (0.00)
Water absorption at saturation (%)	0.19 (0.01)	0.15 (0.05)	0.14 (0.01)	0.04 (0.01)	0.04 (0.00)
Cure ratio (%)	100 (0)	100 (0)	100 (0)	100 (0)	100 (0)
T_g (°C)	125.8 (1.3)	112.8 (2.5)	109.6 (1.5)	105.2 (1.3)	124.8 (4.9)

701

702

703 Table 3. Mechanical properties of the GFRP bars before and after conditioning

Property	**Bar Designation**				
	#3	**#4**	**#5**	**#6**	**#8**
Reference					
Flexural strength, f_u (MPa)	1623.7 (58.2)	1588.1 (93.5)	1757.5 (66.5)	--	1406.3 (151.3)
Interlaminar shear strength, S_u (MPa)	54.7 (1.1)	52.9 (2.1)	55.8 (1.5)	56.0 (0.1)	47.5 (3.7)
Tensile strength, f_t (MPa)	1315.3 (31.1)	1281.5 (35.3)	1237.4 (33.3)	1270.0 (31.4)	1271.0 (29.9)
Tensile modulus, E (GPa)	62.5 (0.4)	61.3 (0.4)	60.0 (1.3)	60.5 (0.5)	61.8 (0.3)
Tensile strain, e	2.3 (0.1)	2.1 (0.1)	2.1 (0.1)	2.1 (0.1)	2.1 (0.1)
Conditioned					
Flexural strength, f_u (MPa)	1440.3 (97.3)	1455.6 (96.4)	1660.0 (62.3)	--	1370.9 (49.9)
Interlaminar shear strength, S_u (MPa)	48.2 (1.5)	50.6 (2.1)	50.2 (2.4)	52.1 (1.8)	47.9 (2.4)
Tensile strength, f_t (MPa)	1251.8 (34.6)	1114.0 (29.4)	1141.1 (41.5)	1095.9 (55.4)	1119.2 (50.0)
Tensile modulus, E (GPa)	63.0 (0.4)	61.9 (0.4)	60.1 (0.2)	60.8 (0.6)	61.7 (0.3)
Tensile strain, e	2.2 (0.1)	1.8 (0.1)	1.9 (0.1)	1.8 (0.1)	1.8 (0.1)

704

705

706 Table 4. Specimen length for the tensile testing of the GFRP bars

Bar Size	Gauge Length (mm)	Anchor Length (mm)	Specimen Length (mm)
#3	465	400	1265
#4	583	510	1603
#5	713	630	1973
#6	848	740	2328
#8	1166	990	3146

707

708 Table 5. Estimated affected portion of the GFRP bars

Affected Portion	#3	#4	#5	#6	#8
Area ($x\ 10^{-3}$ mm^2)	138.2	186.2	270.0	111.7	223.0
Thickness ($x\ 10^{-3}$ mm)	4.4	4.7	5.4	1.9	2.8
% of the nominal diameter	0.05	0.04	0.03	0.01	0.01

709

710

Figure 1 – Tested GFRP bars specimens

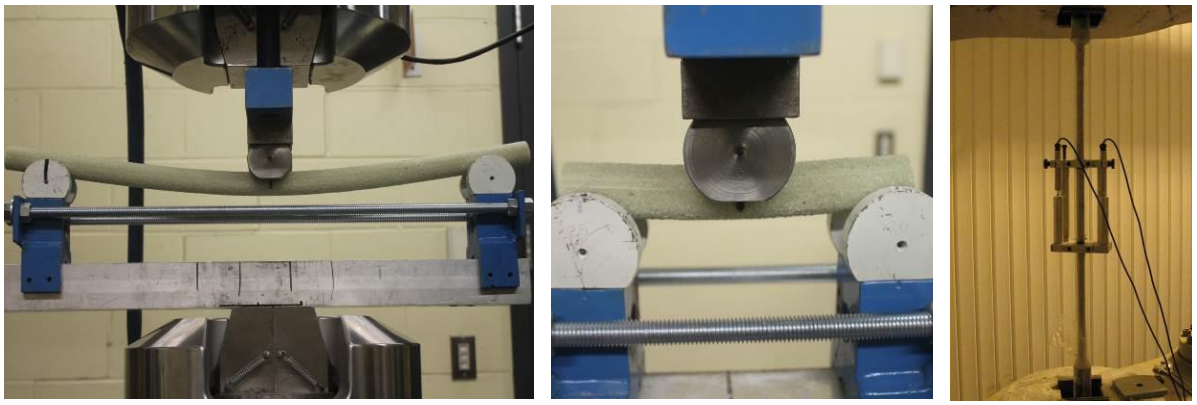

(a) Flexure (b) Short-beam shear (c) Tensile

Figure 2 - Test setup and instrumentation

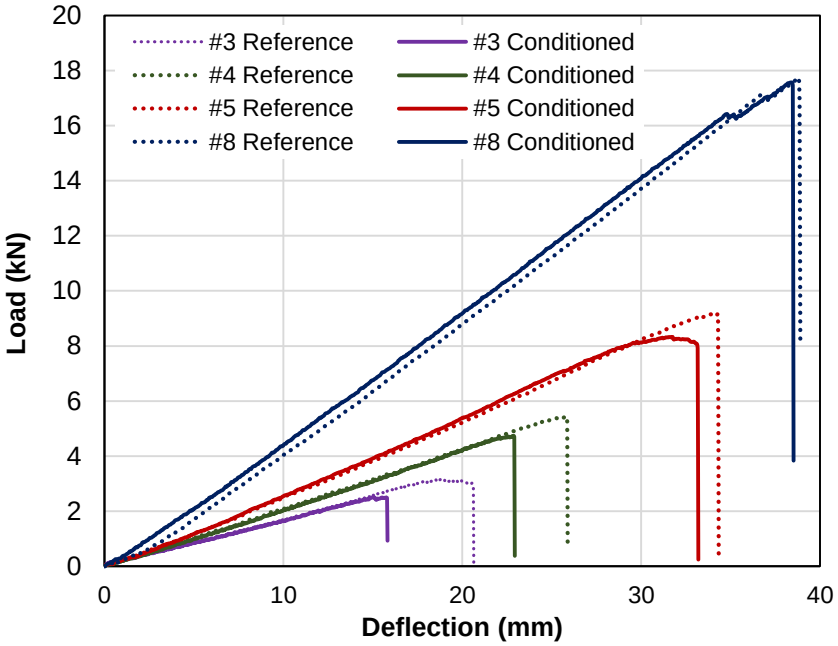

(a) Load and deflection behavior

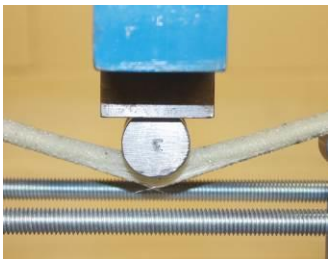

(b) Failure of #3 bars

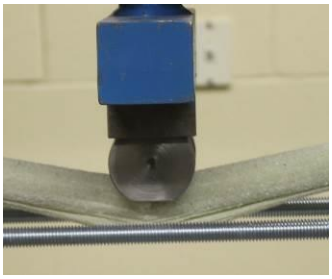

(c) Failure of #8 bars

Figure 3 - Load-deflection and failure behavior of GFRP bars in bending

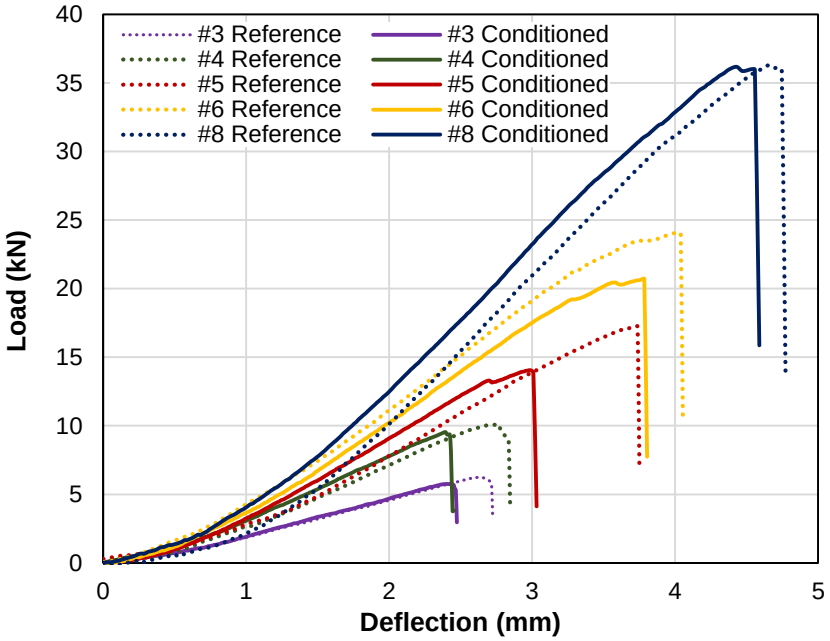

(a) Load and deflection behavior

(b) Failure of #3 bars

(c) Failure of #8 bars

Figure 4 - Load–deflection and failure behavior of the GFRP bars under short-beam shear testing

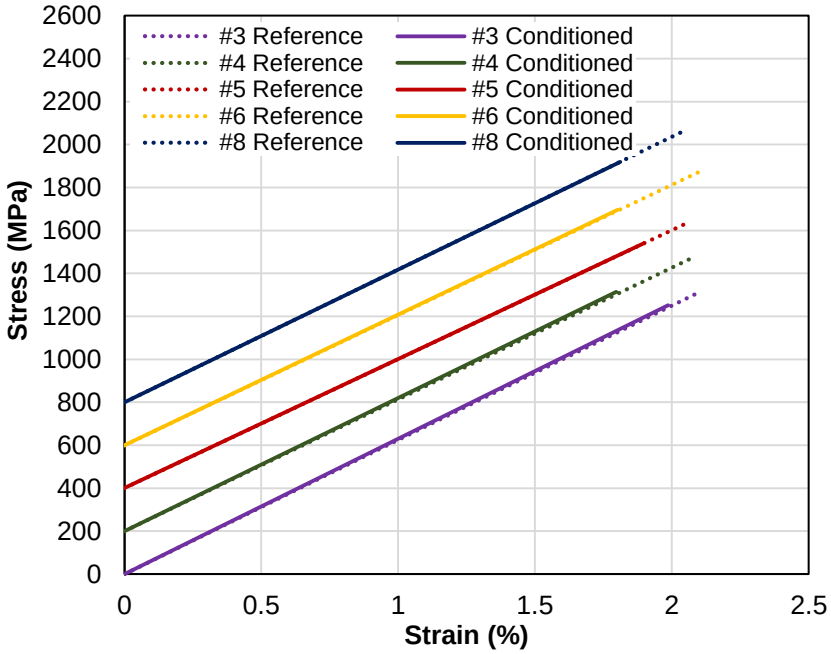

(a) Stress and strain behavior

(b) Failure of #3 bars

(c) Failure of #8 bars

Figure 5 - Stress–strain and failure behavior of the GFRP bars in tension

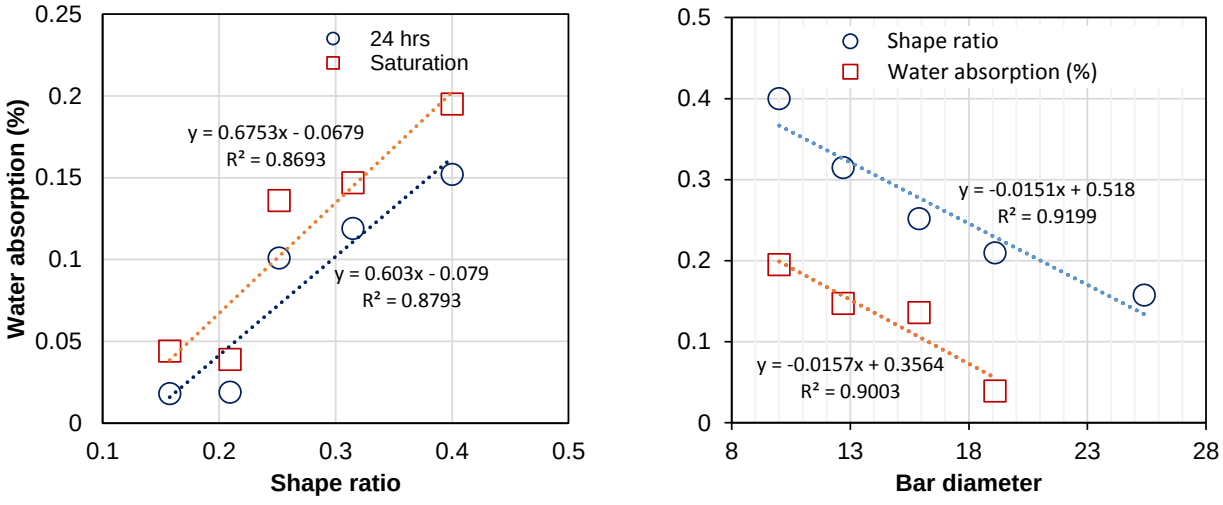

(a) Water absorption and shape ratio (b) Shape ratio and water absorption with bar diameter

Figure 6 - Relationship of water absorption to the shape ratio and bar diameter

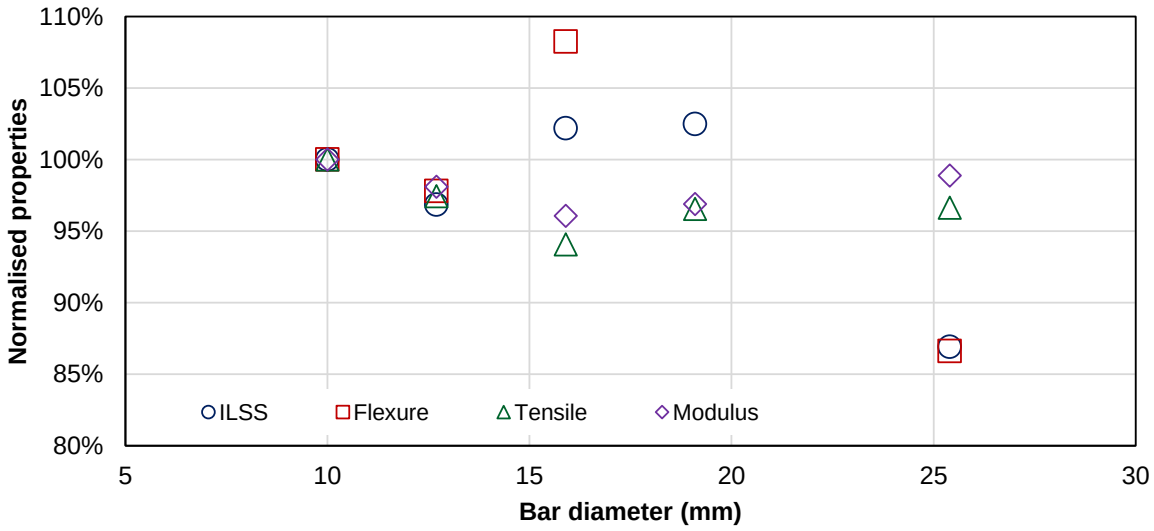

Figure 7 - Normalized mechanical properties of the GFRP bars

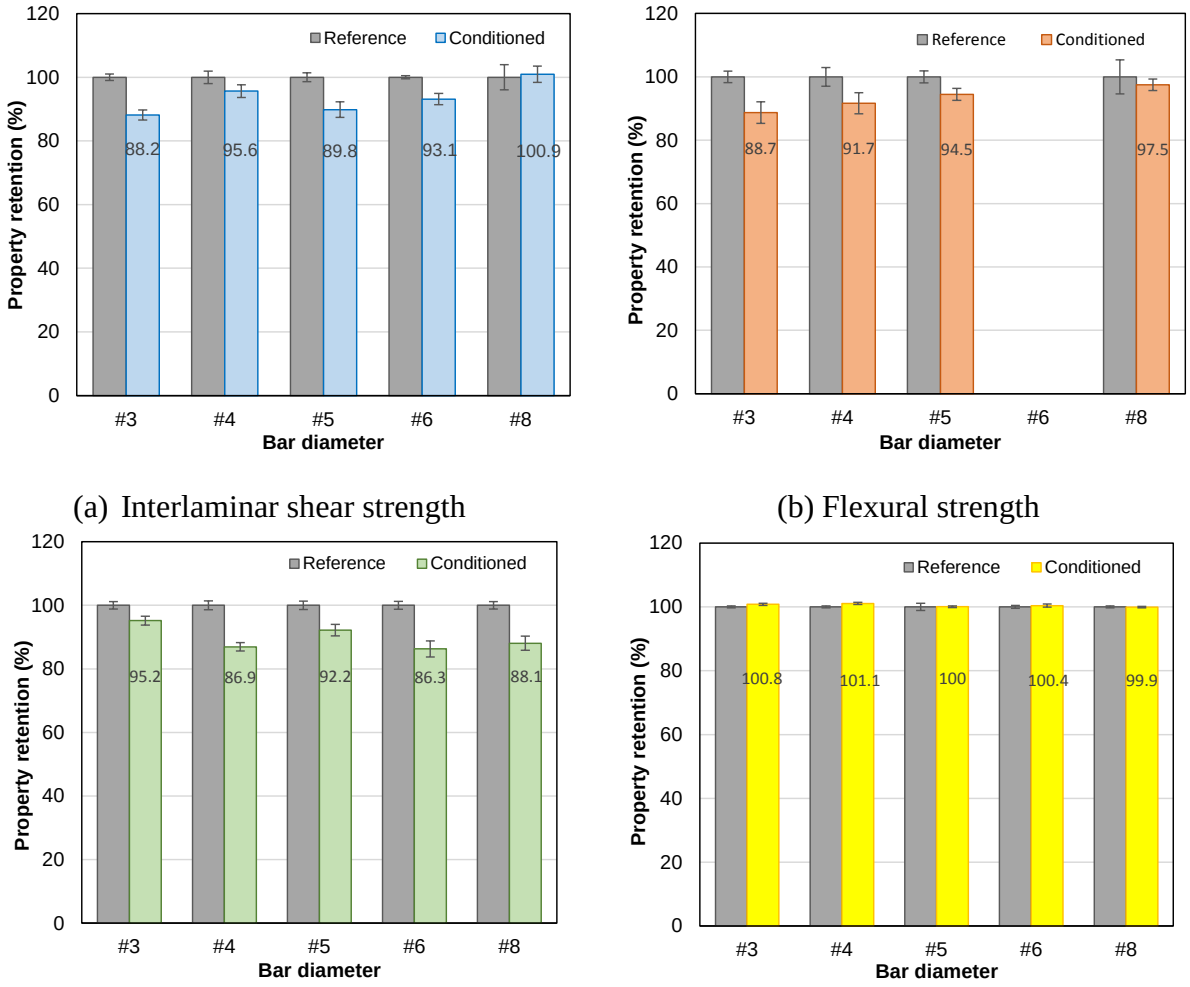

(a) Interlaminar shear strength (b) Flexural strength

(c) Tensile strength (d) Modulus of elasticity

Figure 8 - Property retention of GFRP bars with different diameters

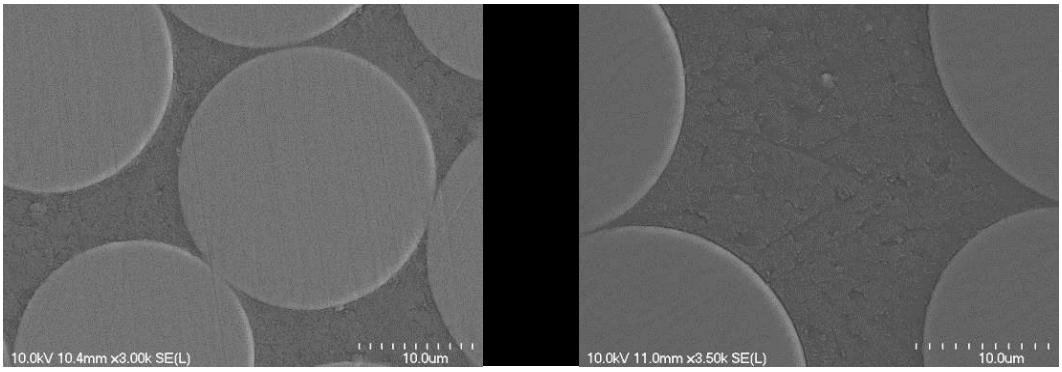

(a) Center of the bar (b) Near surface of the bar

Figure 9 - SEM micrographs of the reference GFRP bars

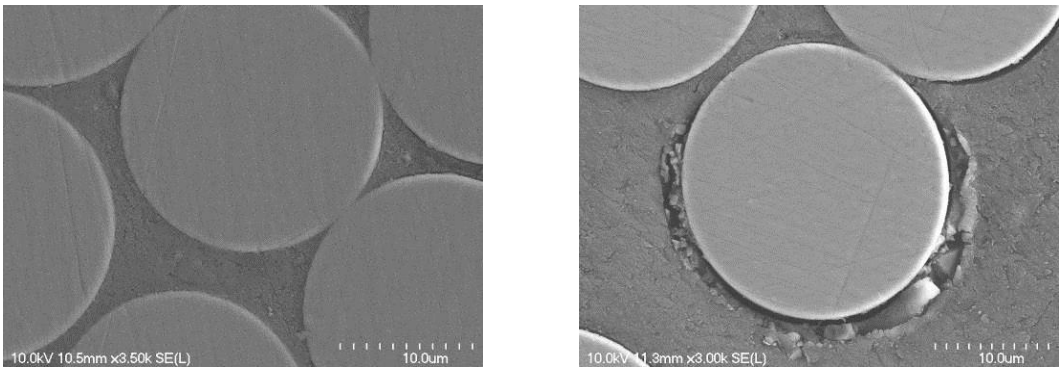

(a) Center of the bar (b) Near surface of the bar

Figure 10 - SEM micrographs of the conditioned GFRP bars

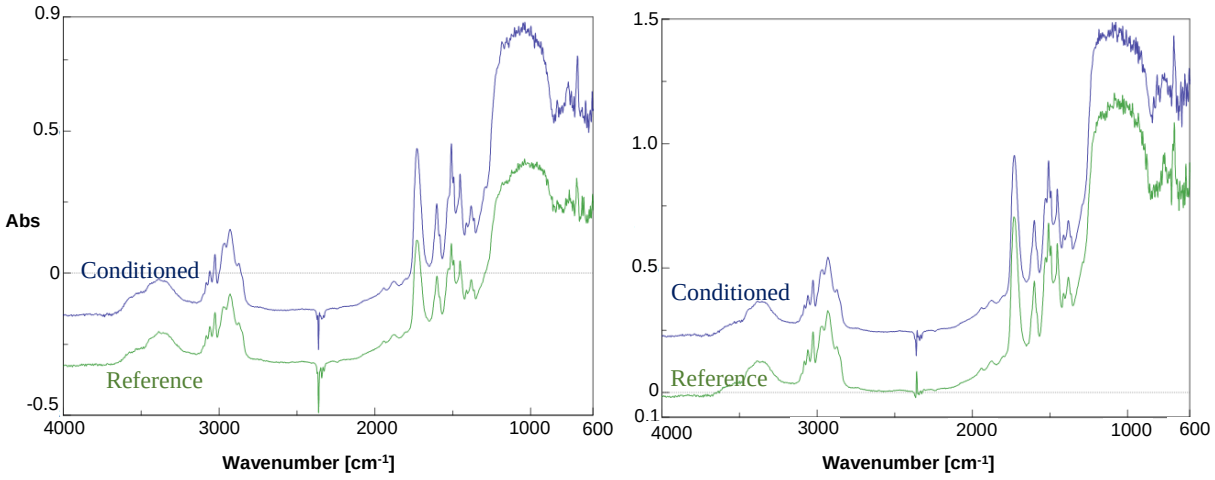

(a) #3 GFRP bars (b) #8 GFRP bars

Figure 11. FTIR spectrum of the GFRP bars before and after conditioning.